Available online at www.sciencedirect.com

ScienceDirect

Energy Procedia 129 (2017) 1018–1025

Energy Procedia

www.elsevier.com/locate/procedia

IV International Seminar on ORC Power Systems, ORC2017
13-15 September 2017, Milano, Italy

Experimental performance evaluation of a multi-diaphragm pump of a micro-ORC system

Gianluca Carraro[a]*, Platon Pallis[b], Aris D. Leontaritis[b], Sotirios Karellas[b], Panagiotis Vourliotis[b], Sergio Rech[a,c], Andrea Lazzaretto[a]

[a] *Department of Industrial Engineering – University of Padova, via Venezia 1, 35131,Padova, Italy.*
[b] *Laboratory of Steam Boilers and Thermal Plants - National Technical University of Athens, 9 Iroon Polytechniou, 15780, Athens, Grece.*
[c] *Interdepet. Center "Giorgio Levi Cases" for Energy Economics and Technology - University of Padova, via Marzolo 9, 35131 Padova, Italy.*

Abstract

The performance of micro-scale ORC systems strongly depends on the performance of their key components. While the heat exchangers and expander have been extensively investigated, the pump has only received limited attention. The main purpose of this work is the experimental characterization of a multi-diaphragm positive displacement pump, integrated in an experimental ORC system with a rated power output of 4kWel. The study focuses on the experimental evaluation of the pump performance and on cavitation phenomena. A detailed presentation of the experimental procedure and results is supplied. A great effort has been spent in calculating the global and volumetric pump efficiencies for a wide range of operational conditions, which reach maximum values around 45-48% and 95%, respectively. With regards to cavitation issues, the effect of the available Net Positive Suction Head at the pump inlet has been deeply investigated both at partial and full load to obtain guidelines for stable operation. Finally, an extensive dataset of steady-state operating points has been used to calibrate an improved version of a semi-empirical model previously developed for positive displacement ORC pumps. Special attention has been given to the ability of the model to accurately predict the behaviour and performance of the pump at different, properly chosen, steady-state conditions. Relative errors in between 0.5%, for the outlet temperature, and 10%, for the electric power consumption, are achieved.

Peer-review under responsibility of the scientific committee of the IV International Seminar on ORC Power Systems.

Keywords: micro-ORC system; multi-diaphragm pump; experimental investigation

* Corresponding author. Tel.: +39-049-8276747; fax: +39-049-8276785.
*E-mail address:*gianluca.carraro.4@studenti.unipd.it

1876-6102
Peer-review under responsibility of the scientific committee of the IV International Seminar on ORC Power Systems.
10.1016/j.egypro.2017.09.232

1. Introduction

The exploitation of the waste heat from engines or industrial processes may significantly contribute to power production. The ORC system is an effective solution to generate power from low temperature waste heat due to the thermodynamic properties of the organic fluids that can match better than water with these sources. The ORC system size may range from some megawatts (e.g., in geothermal applications) to few kilowatts (e.g., heat recovery from small internal combustion engines). Here the focus is on the latter, in which the intrinsically low efficiency deriving from the low temperature sources is further penalized by the low efficiency of the necessarily simple and cheap components. So, one of the most important design challenge consists in reducing inefficiencies while keeping low costs. Micro-scale ORC systems have been given relatively low attention in the literature and most of the existing experimental studies focus on the evaluation and improvement of expander efficiency. Nevertheless, in such small systems, the low efficiency of the pump heavily affects both net power output and overall efficiency of the cycle, making it a key component along with expander and heat exchangers [1, 2]. Another issue regarding pump operation is the cavitation occurrence. Cavitation causes an increase of vibration and noise level, drop of delivered flow rate and/or pressure head, efficiency drop and eventually the collapse of the system operation. It can also cause damage to the pump elements, which can even result in pump failure. In addition, the poor literature background on ORC pumps underlines the need for further research on this field. Only a few experimental studies are completely dedicated to pumps in small-scale ORC systems. Lin [3] has conducted an experimental study on seven pumps, including piston, plunger as well as power steering pumps in order to select the most suitable solution for a 1 kW solar ORC system. The maximum measured efficiencies (based on mechanical power) range from 31% to 81%. However, incorporating the motor efficiency, other researchers have shown low global efficiencies of ORC pump systems. Bala et al. [4] studied the influence of different working fluids on the overall efficiency of sliding-vane refrigerant pumps, reaching 18% for R113 and only 12% for R11. Quoilin et al. [5] reported an overall ORC pump isentropic efficiency of 25% in a 2 kW ORC unit. Declayé [2] has deeply investigated the global and volumetric efficiency, as well as the cavitation issue of five types of volumetric pumps suitable for micro-ORC systems, including mono/multi-diaphragm, gear, piston and plunger pumps. The most favourable was the plunger pump, with a global efficiency of 46.6%. at nominal speed decreasing at lower speeds.

In this context, the goal of this work is the experimental performance evaluation of a multi-diaphragm pump integrated in a micro-scale ORC system having a rated power output of 4 kW. An experimental campaign was properly planned to create an ORC system setup which makes a sufficient number of pump operating points available in the whole range of operation. Particular attention is also payed to the search for the operating condition leading to cavitation and to the system reaction to this phenomenon. The experimental results are also used to validate and improve a semi-empirical model of the pump, previously developed by D'Amico et al. [6].

2. The test rig and the experimental strategy

2.1. The ORC prototype unit

Figure 1 shows a schematic of the ORC prototype unit including the main measuring equipment. It is a conventional low-temperature subcritical Organic Rankine Cycle using R134a as working fluid designed as a waste heat recovery system for the jacket water of marine diesel auxiliary internal combustion engines (ICEs), simulating the jacket water with a natural gas boiler. The hot water temperature reaches about 90°C and the heat input is in the order of 90 kWth. The high-pressure vapour is expanded in two parallel scroll expanders which are actually two open-drive automotive scroll compressors working in reverse operation. Each expander drives an asynchronous generator by means of a belt-pulley, transferring the power at the same rotational speed (ratio 1:1). The generators are connected to the 50Hz/400V electrical grid via a regenerative inverter module, which controls the rotational speed of the generators, and in turn of the expanders. With regards to the pump system, the liquid receiver after the condenser is followed by a tube-in-tube heat exchanger fed by an external heat pump delivering cold water at an adjustable flow rate and temperature. This allows imposing a given degree of subcooling at the pump suction line to prevent and study cavitation issues. The pump is a volumetric multi-diaphragm pump (Hydra Cell, model G-10X) and raises the fluid pressure at about 22-25 bar, depending on the operational conditions. The pump is connected to a 960 rpm (nominal speed at 50 Hz) induction motor driven by a variable speed drive (VSD).

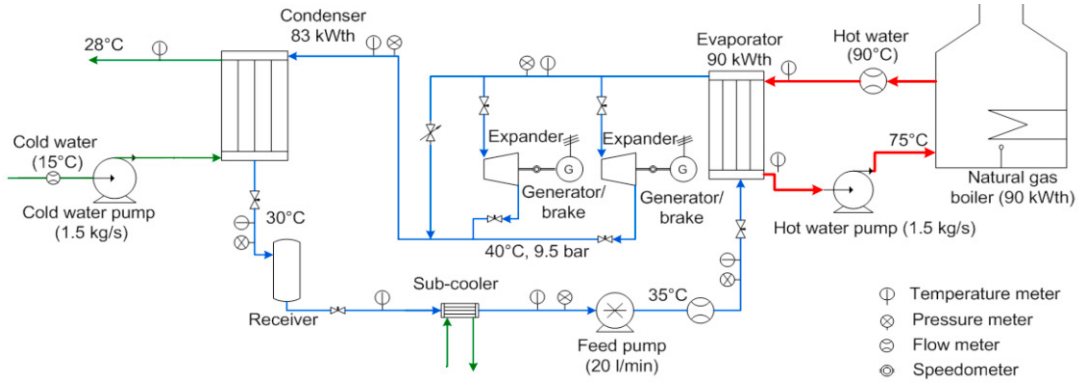

Fig. 1: Schematic diagram of the ORC prototype unit (the values of the main parameters are referred to the design point)

Tab. 1: Features of the installed meters

Meter type	Manufacturer	Meter model	Accuracy
Energy meter	DUCATI SpA	DUCA-LCD96	± 1%
Flow meter	KROHNE GmbH	OPTIMASS MFS 1000 S25	± 0.2 %
Temperature meter	WIKA Srl	PT100 0..+200C4/20MA10/30VD 0+100C	± 0.3 °C
Pressure meter	WIKA Srl	S-10 abs G1/2 4/20MA	± 0.1 bar

2.2. The experimental campaign

The pump performance is assessed by including the experimental data in two categories of operating conditions:
A. Variable pressure difference (Δp) between inlet and outlet at constant rotational speed (i.e. constant $\dot{m}$)
B. Variable rotational speed (rpm) at constant pressure difference (Δp).
Moreover, the desired Δp in category A is obtained by means of two different approaches:
1st approach - constant outlet pressure of the pump (cycle maximum pressure) and variable inlet pressure;
2nd approach - constant inlet pressure and variable outlet pressure.

During the experiment sessions, three main parameters have been controlled to achieve the desired operating conditions of the pump: a) the low-pressure of the cycle via the condenser cooling water flow (an increase/decrease of the water flow entails a decrease/increase of the pump inlet pressure, p_{in}, and temperature, T_{in}), b) the pump rotational speed and in turn the delivered mass flow rate, via the VSD of the pump motor, and c) the high pressure of the cycle via the rotational speed of the scroll expanders (for a given mass flow rate, an increase/decrease of the expander rotational speed causes a decrease/increase of the scroll inlet pressure, which is the maximum pressure of the cycle). The latter allows for the effective control of the pump outlet pressure (p_{out}). The sub-cooling degree has been kept constant by adjusting the flow rate and the temperature of the water supplied to the sub-cooler. On the other hand, in the cavitation study the subcooling degree has gradually been decreased to achieve cavitation conditions (Section 3.2).

Performance parameters of the pump are the global and the relative volumetric efficiencies, defined as

$$\eta_{glob} = \frac{\dot{W}_{hyd}}{\dot{W}_{mot}} \qquad \eta_{vol,rel} = \frac{\dot{V}}{\dot{V}_{th}} \cdot \frac{\dot{V}_{th}}{\dot{V}_{manu}} = \frac{\dot{V}}{\dot{V}_{manu}} \tag{1a,b}$$

where $\dot{W}_{hyd}$ is the hydraulic power delivered to the fluid and $\dot{W}_{mot}$ is the electric power of the motor. Moreover, $\dot{V}$ is the actual volume flow rate delivered by the pump, $\dot{V}_{manu}$ is the volume flow rate that the pump should deliver according to the characteristic curves provided by the manufacturer [7] and $\dot{V}_{th}$ is the theoretical volume flow rate, as derived from the swept volume and rotational speed of the pump. It is important to remember that the proper "volumetric efficiency is defined as the ratio between the actual volume flow rate ($\dot{V}$) and the theoretical one ($\dot{V}_{th}$). However, manufacturers do not usually provide accurate data about the swept volume of the pumps; therefore, the relative volumetric efficiency is used in this work. The same definition is also used in [2]. Hereafter "volumetric efficiency" is always used for simplicity but actually it stands for "relative volumetric efficiency".

Concerning the pump operation, the phenomenon of cavitation is analysed. To avoid cavitation it is necessary to maintain the minimum liquid pressure in the pump always sufficiently higher than the saturation pressure at the inlet temperature. The difference between the two pressures is called available *Net Positive Suction Head* (*NPSH*):

$$NPSH_a = p_{in,pp} - H_a - Pvp \quad (2)$$

where: $p_{in,pp}$ = pressure at pipe inlet; H_a = acceleration head at pump suction; Pvp = absolute vapour pressure of liquid at pumping temperature. Note that Eq. (2) does not include the vertical distance from the surface of the liquid to the pump centre line and friction losses in suction line, being $p_{in,pp}$ measured at pump inlet.

The term H_a can be evaluated from the technical data sheet of the pump [7], where the required head (*NPSHr*) to ensure cavitation free operation is also provided. Thus, the condition of non-cavitation is $NPSH_a > NPSH_r$.

Among the different approaches to avoid cavitation ([see, e.g., 1,8]), thermal subcooling is chosen to reduce *Pvp* and keep, in turn, *NPSHa* sufficiently higher than *NPSHr* in any operation condition.

3. Experimental results and discussion

Results of the experimental tests on pump performance and cavitation are discussed next. The evaluation of pump efficiencies follows the outline presented in Section 2.2, which separates the calculation into the two categories (A and B). Cavitation tests provide useful information for the integration of this type of pump in micro-scale ORC systems.

3.1 Pump efficiencies

Global and volumetric pump efficiencies obtained at constant rotational speed and variable pressure difference (Δp) (category A in Section 2.2) are shown in Fig. 2. The influence of the two different approaches (constant outlet pressure and variable inlet pressure, and vice versa) is also pointed out. An increasing trend of the global efficiency with Δp can be observed in all cases (as also reported in [2]) independently of the followed approach, which is apparent from the 26.5Hz curves (Fig. 2 (a)). At this lower frequency, the global efficiency varies from 15% to 24% for a Δp that ranges from 7 to 15.5 bar. A strong improvement in the efficiency is found when switching from 26.5 to 36.5 Hz. At 36.5 Hz the efficiency varies between 39 – 48% a for a Δp ranging between 11 and 17 bar. A further increase of the rotational speed results in a slight decrease of the global efficiency, as indicated by the 46.5Hz curve.

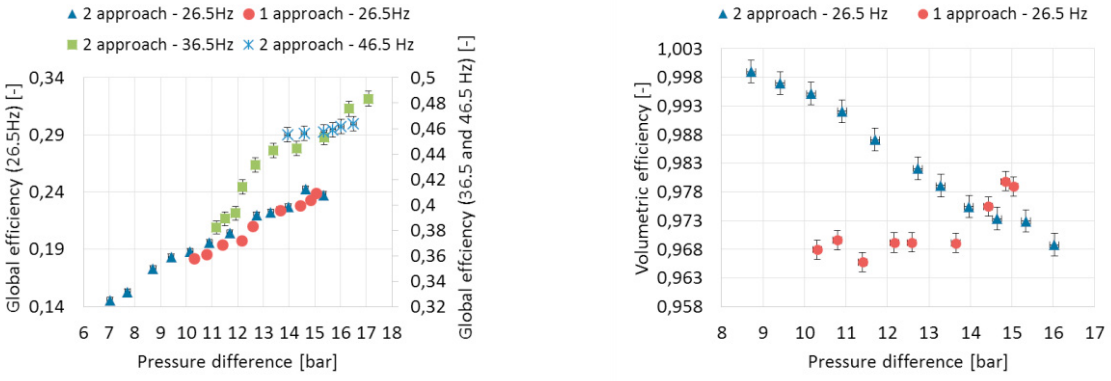

Fig. 2: a) Global and b) Volumetric pump efficiencies vs pressure difference using the two approaches of category A in Section 2.2

The volumetric efficiency on the other hand (Fig. 2 (b)) is strongly affected by the followed approach. The expected trend is a decrease of the volumetric efficiency with the increase of the pressure difference as shown in [2]. Nevertheless, this trend is well recognized only from the points of the second approach, whilst the results of 1st approach do not follow any clear trend and are quite scattered. An explanation for this behaviour can be found in the

applied procedure during the 1st approach tests. A change to the inlet pressure (the maximum pressure is kept constant) involves a change in the effectiveness of the cooling circuit.

In particular, an increase of the cold-water flow rate in the condenser leads to a decrease of temperature and pressure of the working fluid that, as a result, enters the pump with a higher density and higher mass flow rate, considering the same volume flow rate at the pump suction. Keeping the inlet conditions constant and varying only the outlet pressure (2nd approach) is a much more stable procedure since it does not affect the pump inlet conditions. The results are in agreement with those presented in [2], where the values of the volumetric efficiency for a multi-diaphragm pump are usually above 95% and decrease gradually with the increase of the pressure difference.

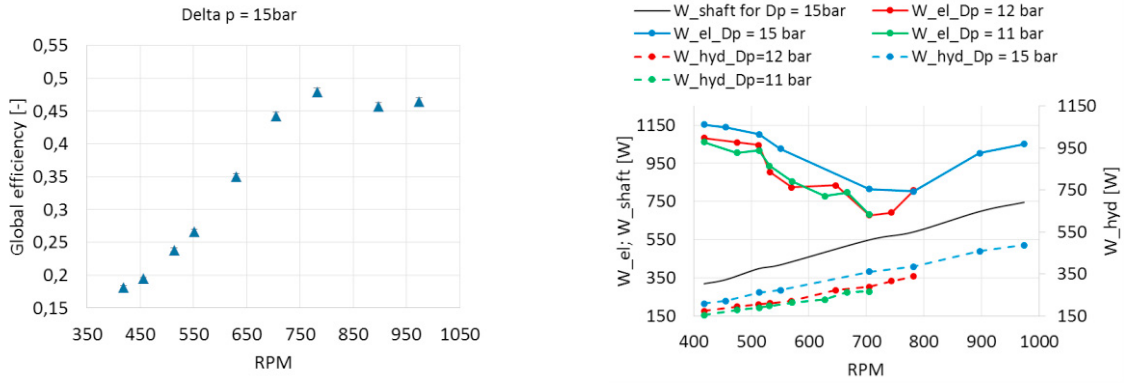

(a) (b)

Fig. 3. a) Global efficiency vs RMP for a pressure difference of 15 bar and b) motor, hydraulic and pump shaft power for different Δp

The trend of the global efficiency under variable pump speed (rpm) for a constant pressure difference of 15bar is in turn presented in Fig. 3 (a). An efficiency peak is observed at 782 rpm (f = 40Hz). This trend agrees with the electric power consumption of the motor versus the rotational speed shown in Fig. 3 (b), where a hollow in the mid-range of 700-800rpm can be seen. The hydraulic power delivered to the fluid by the pump increases linearly with the rotational speed and the pressure difference, being defined as the product between volume flow rate ($\dot{V}$) and pressure difference (Δp). Indeed, the volume flow rate is a linear function of the rotational speed (RPM). This is apparent from the curves provided by the manufacturer [7]. The shaft power required by the pump is not directly measured but is evaluated by the following equation provided by the pump manufacturer [7]:

$$\dot{W}_{sh,pump}[kW] = \frac{\dot{V}\Delta p}{511} + \frac{15 \cdot rpm}{84428} \tag{3}$$

This power shows a similar trend (linear) to the hydraulic power, as expected (see the black line in Fig. 3 (b), where the only curve at Δp=15 bar is shown for clarity). The electric power consumption of the pump system (W_{el}) shows instead a minimum around 700 rpm for every value of Δp.

Note that the absorbed electric power of the motor in the low-frequency range is higher than at nominal frequency (50 Hz) because the motor works at very low load (<33%) and efficiency in each test, which become even lower at low-frequency operation (f<35 Hz). Moreover, the manufacturer of the energy meter ensures high accuracy for AC currents above 35Hz, and the effect on the motor of higher order harmonics generated by the VSD is not considered, although it could affect both measurements and motor operation.

3.2 Cavitation tests

Cavitation is enforced under both partial (f=28 Hz) and full load (f=50Hz) operation. The criterion used to detect cavitation is a 5% volumetric flow rate drop. Figure 4 (a) clearly shows that the threshold cavitation value of NPSH is higher at full load than at partial load (lower rpm). This difference between the two values is in agreement with the increase of *NPSHr* with the rotational speed already shown by the manufacturer [7] and Leontaritis et al. [9]. A similar trend is also found in [2]. Cavitation is achieved by increasing the pump inlet temperature, and in turn *Pvp*, by decreasing the subcooling degree. This in turn results in a decrease of NPSHa (Fig. 4 (b)).

As soon as NPSHa reaches the critical value (≈*NPSHr*), cavitation is initiated. As a result, a synchronized drop of mass flow rate, *NPSHa* and outlet pressure is registered. On the other hand, cavitation affects the inlet pressure, *Pvp* and the inlet temperature with higher or lower delays, which are caused by the inertia and damping action of the receiver between the condenser outlet and pump inlet. In particular, the inlet temperature starts decreasing after the receiver is cooled down. This process is slow due to the low mass flow rate circulating in the system, regardless of the low refrigerant temperature after the condenser. After the full load cavitation test, a stable operation is recovered by increasing the subcooling degree. Pressure and temperature variations in cavitation tests are shown in Fig. 4 (b).

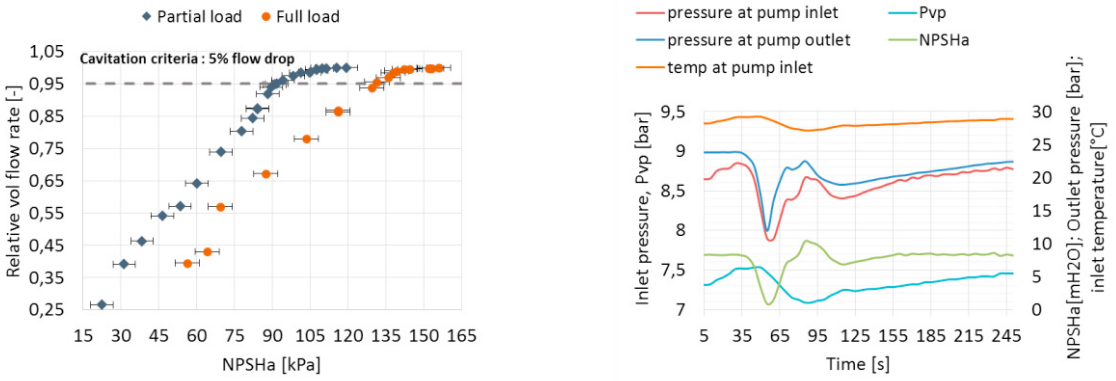

(a) (b)

Fig. 4: a) Relative volume flow rate vs. *NPSHa* and b) pressure and temperature variation during cavitation tests

4. Semi – empirical pump modeling

The semi-empirical model of the pump is built in accordance with the structure proposed by D'Amico et al. [6] which, differently from those previously proposed in the literature (see for example Winandy et al. [10], and Quoilin et al. [5]), considers the fluid trapped into the dead volume. A subdomain of the dataset obtained by the experiments (Section 3) is used to calibrate the model. The points in this subdomain have been accurately chosen to cover the whole operating range of the pump. Consequently, the predictive capability of the calibrated model is assessed using the rest of the experimental domain. The main features of the model, calibration procedure and simulation results are shown in the following.

4.1. Modelling approach

Three partially superimposed sets of simple thermodynamic processes (Fig. 5) are used to depict the pump behavior. Each set is carried out by i) the main stream delivered by the pump (black), ii) the stream re-circulating through clearances (red – called here "leakage") and iii) the trapped stream in the dead volume (grey). The respective thermodynamic processes, the model equations of each of them and the mass and energy balance equations are described in [6]. The main and trapped mass flow rates are evaluated from the following geometrical parameters:

- the swept volume (V_H);
- the ratio between maximum (V_S) and dead (V_0) volumes ($C = V_0/V_s$);
- the ratio between volume when the inlet valves open (V_1) and dead volume ($f_e = V_1/V_0$);
- the ratio between volume when the outlet valves open (V_{ex}) and maximum volume $\left(f_p = V_{ex}/V_S\right)$.

The re-circulating mass flow rate is calculated considering an isentropic adiabatic expansion through a converging nozzle having a minimum cross-sectional area of $A_{leak,nom}$. Isentropic adiabatic flows in nozzles having minimum cross sectional areas of A_{su} and A_{ex} are also considered to estimate the supply and discharge pressure drops (processes $su \rightarrow su_1$ and $ex_1 \rightarrow ex_2$), respectively. The heat transfer between the working fluid and the suction and delivery ducts ($\dot{Q}_{su}$and $\dot{Q}_{ex}$), and between ducts and environment ($\dot{Q}_{amb}$ in Fig. 5) are computed using the $\varepsilon - NTU$ method equations that include the product between the contact area and the overall heat transfer coefficient involved in each process ($AU_{su,nom}$, $AU_{ex,nom}$ and AU_{amb}, respectively). The mechanical losses ($\dot{W}_{loss}$) in all bearings are lumped into a unique mechanical loss torque ($\dot{W}_{loss} = T_{mech} \cdot \omega$) and they are assumed to be dissipated in the environment as heat.

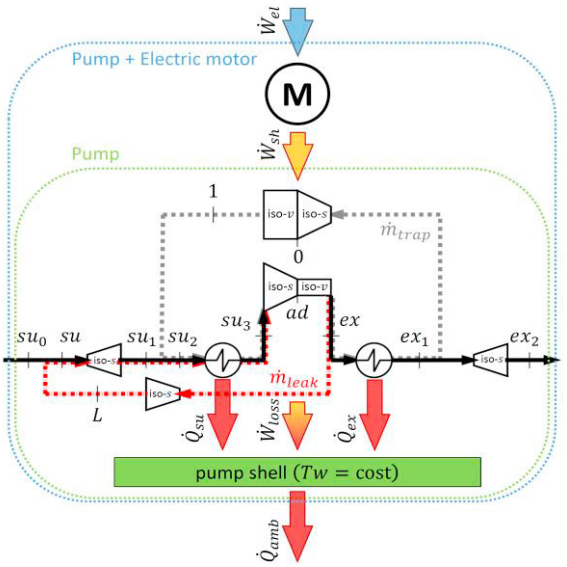

Fig. 5: Thermodynamic processes used to describe the behaviour of the pump and electric motor

Table 2: Calibrated values of the model parameters ($\mathbf{x}_i$*).

Model parameter	Calibrated value
$AU_{amb}[W/K]$	0.986
$AU_{ex,nom}[W/K]$	50
$AU_{su,nom}[W/K]$	60
$A_{ex}[m^2]$	0.00101
$A_{su}[m^2]$	0.0007002
$A_{leak,nom}[m^2]$	$4.8E-07$
C [−]	0.1305
$V_H[m^3]$	0.00002197
$f_p[-]$	0.9984
$f_e[-]$	1.027
$T_{mech}[N \cdot m]$	4.251

Finally, the efficiency of the electric motor (Fig. 5) is evaluated with a 4th grade polynomial function:

$$\eta_{mot} = \frac{W_{sh,pump}}{W_{el}} = f(N, Load) = \\ = -5.31247914 \cdot 10^{-2} \cdot N + 1.22264560 \cdot 10^{-4} \cdot N^2 - 1.18454157 \cdot 10^{-7} \cdot N^3 + 4.13550565 \cdot 10^{-11} \cdot N^4 + \\ +1.509897 \cdot 10^{1} \cdot Load - 1.44009810 \cdot 10^{2} \cdot Load^2 + 6.45006093 \cdot 10^{2} \cdot Load^3 - 1.04246533 \cdot 10^{3} \cdot Load^4 \\ +7.9110469\,, \tag{4}$$

where N is the rotational speed in RPM and $Load$ is the ratio between the delivered mechanical power and the nominal electric power of the motor. Equation (4) derives from a regression of the motor efficiency values calculated for some experimental points that were chosen to carry out the calibration procedure (see Section 4.2). In particular, the efficiency is evaluated as ratio between shaft power (Eq. (3)) and measured electric power absorbed by the motor. This empirical equation has been adopted on grounds of the trend of the measured electric power with the rotational speed (Fig. 3 (b)). In its support, the dependence of the motor efficiency on the imposed frequency is not provided by the manufacturer [11].

4.2. Calibration and simulation results

The semi-empirical model of the pump is calibrated using fourteen selected sets of values of the following pump operating variables: rotational speed (N), pressures and temperatures at pump inlet (p_{su_0} and T_{su_0}) and outlet (p_{ex_2} and T_{ex_2}), mass flow rate at pump outlet ($\dot{m}_{ex_2}$), and electric power consumption ($\dot{W}_{el}$) which were measured at different operating points. The calibration of the model consists of an optimization procedure which searches for the values of the model parameters xi $\left(AU_{amb}, AU_{ex,nom}, AU_{su,nom}, A_{ex}, A_{su}, A_{leak,nom}, V_H, C, f_p, f_e, T_{mech}\right)$ that minimize the error $\left(f(x_i)\right)$ between the experimentally measured and the calculated values of the operating variables $\dot{m}_{ex_2}$, $\dot{W}_{el}$ and T_{ex_2} for fixed values of the remaining operating variables (T_{su_0}, p_{su_0}, p_{ex_2} and N). The error $f(x_i)$ is computed as:

$$f(x_i) = \sqrt{\sum_{j=1}^{14}\left(\frac{\dot{m}_{ex_2,calc} - \dot{m}_{ex_2,meas}}{\dot{m}_{ex_2,meas}}\right)_j^2} + \sqrt{\sum_{j=1}^{14}\left(\frac{\dot{W}_{el,calc} - \dot{W}_{el,meas}}{\dot{W}_{el,meas}}\right)_j^2} + \sqrt{\sum_{j=1}^{14}\left(\frac{T_{ex_2,calc} - T_{ex_2,meas}}{T_{ex_2,meas}}\right)_j^2} \tag{5}$$

The calibration procedure was carried out by means of the variable metric method available in EES® software [12]. Table 2 lists the obtained optimum values of the model parameters. The maximum relative errors (Fig. 6) result to be lower than that obtained in [6], and they are 4% for the outlet mass flow rate, 4% for the pump shaft power, 10% for

the electric power and 0.5% for the outlet temperature. Unlike other works in the literature, we did not include in the calibration procedure all the available experimental data to test the model accuracy for different points from those used in the calibration itself. Figure 6 shows the capability of the model in predicting the measured values both used (blue triangles) and not used (red points) in the calibration procedure.

Due to the rough empirical model used for the motor efficiency, a higher error in the prediction of the electric power is observed (10% using calibration points and 12.5% using the other points – Fig. 6). The simulation results show a very good accuracy in the prediction of the shaft power (maximum error 4%). This outcome confirms the main purpose of the model section of this work: the development of a model that, first of all, can accurately simulate the operation of the pump itself, regardless of the motor operation.

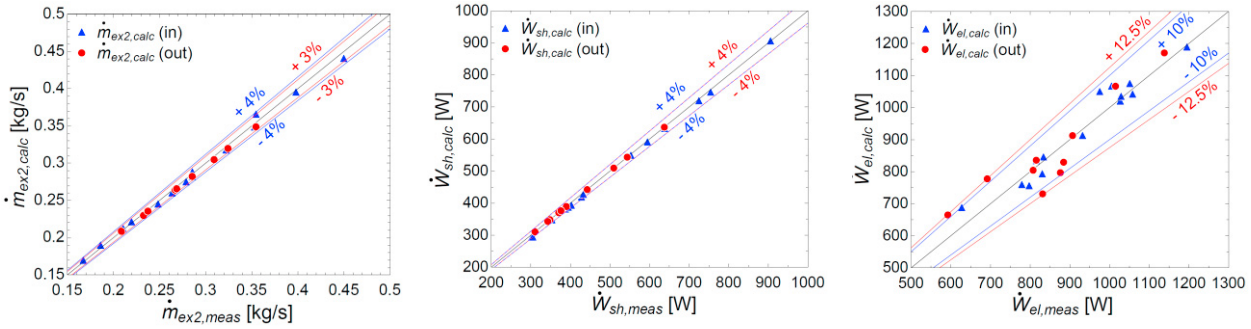

Fig. 6: Comparison of a) mass flow rate, b) shaft power and c) electric power between points in (*in*) and out (*out*) of calibration procedure.

5. Conclusions

The operation of a multi-diaphragm pump integrated into a micro-scale ORC has been investigated in this work. Both experimental characterization and modelling simulation have been carried out. For operational conditions at f >36Hz, global efficiencies of about 45 – 48% are achieved. These values are much higher than those reported in other studies for the same type of positive displacement pump [1,2]. Cavitation tests revealed that a *NPSHa*>90.9 kPa at partial load and a *NPSHa*>129.4 kPa at full load are necessary to guarantee operation stability. The semi-empirical model of the same pump developed in [6] has been improved and recalibrated, including also the motor in the pump system. The low efficiency of the electric motor pushes towards a further analysis of its behavior. For this purpose, the installation of a torque meter between motor and pump can improve the estimate of motor consumption and efficiency at different loads and rotational speeds. On the other hand, the model shows a good capability in predicting the main operating parameters of the pump for the whole set of measured values. The maximum relative errors in the calibration procedure are 4% for the outlet mass flow rate, 4% for the pump shaft power, 10% for the electric power consumption and 0.5% for the outlet temperature.

References

[1] Quoilin S, Broek MVD, Declaye S, Dewallef P, Lemort V. Techno-economic survey of Organic Rankine Cycle (ORC) systems. Renewable and Sustainable Energy Reviews. 2013;22:168-86.
[2] Declaye S, Lemort V. Improving the performance of micro-ORC systems [Phd thesis]: Universite de Liege, Liege, Belgium.; 2015.
[3] Lin C. Feasibility of using power steering pumps in small-scale solar thermal electric power systems. [Bachelor Thesis]: MIT; 2008.
[4] Bala EJ, O'Callaghan PW, Probert SD. Influence of organic working fluids on the performance of a positive-displacement pump with sliding vanes. Applied Energy. 1985;20:153-9.
[5] Quoilin S, Lemort V, Lebrun J. Experimental study and modeling of an Organic Rankine Cycle using scroll expander. Applied Energy. 2010;87:1260-8.
[6] F. DA, Pallis P, Leontaritis AD, Karellas S, Kakalis NM, Rech S, et al. Semi-empirical model of a multi-diaphragm pump in an Organic Rankine Cycle test rig. 4th International Conference on Contemporary Problems of Thermal Engineering, September 14-16. Katowice, Poland.2016.
[7] Wanner Engineering I. Hydra-Cell® INDUSTRIAL PUMP – Installation & Service Models: D-10 and G-10, D10-991-2400B5/2004.
[8] Schuster A, Sichert A, Aumann R. Thermodynamic machine and method for the operation thereof. F01K 25/08 (20060101); F01K 25/00 (20060101); F01K 13/00 (20060101); ed: Orcan Energy GmbH, Munich (DE); Feb 11, 2014.
[9] Leontaritis AD, Pallis P, Karellas S, Papastergiou A, Antoniou N, Vourliotis P, et al. Experimental study on a low temperature ORC unit for onboard waste heat recovery from marine diesel engines. 3rd International Seminar on ORC Power Systems. Brussels, Belgium.2015.
[10] Winandy E, Saavedra OC, Lebrun J. Simplified modelling of an open-type reciprocating compressor. Int. J. of Th. Sciences 2002;41:183-92.
[11] Motors VH. Valiadis Tests report. Available at http://www.valiadis.gr/?viewp=213.
[12] Klein S. Engineering Equation Solver (EES). Middleton, WI: F-Chart Software; 2008.